RSC Advances

ROYAL SOCIETY OF CHEMISTRY

www.rsc.org/advances

RSC Advances
RSCPublishing

ARTICLE

Polyaniline-Wrapped 1D $CoMoO_4.0.75H_2O$ Nanorods as Electrode Materials for Supercapacitor Energy Storage Application

Cite this: DOI: 10.1039/x0xx00000x

Manas Mandal,[a] Debasis Ghosh,[a] Soumen Giri,[a] Imran Shakir,[b] and Chapal Kumar Das*[a]

Received 00th January 2012,
Accepted 00th January 2012

DOI: 10.1039/x0xx00000x

www.rsc.org/

In this study, a simple and cost effective one pot hydrothermal process has been carried out for the synthesis of 1D $CoMoO_4.0.75H_2O$ nanorod and a binary composite of $CoMoO_4.0.75H_2O$/PANI has also been synthesized by *in situ* oxidative polymerization of aniline with the virgin $CoMoO_4.0.75H_2O$. Two types of PANI morphology have been demonstrated, amorphous nanodimentional PANI uniformly coated on $CoMoO_4.0.75H_2O$ nanorod and interconnected hollow sphere like PANI inside the bulk material. The prepared $CoMoO_4.0.75H_2O$/PANI composite was characterized by X-ray diffraction analysis and Fourier transform infrared spectroscopy for the phase and formation. The surface morphology was investigated by using FESEM and TEM which revealed the formation of $CoMoO_4.0.75H_2O$/PANI composite. The electrochemical characterization of the pseudocapacitive $CoMoO_4.0.75H_2O$ and $CoMoO_4.0.75H_2O$/PANI composites in 1 M Na_2SO_4 showed highest specific capacitance of 285 F/g and 380 F/g, respectively at a current density of 1 A/g. The cyclic stability test demonstrated the specific capacitance retention of about 90.4% after 1000 consecutive charge discharge cycles at 1 A/g constant current density, which is also higher than the virgin $CoMoO_4.0.75H_2O$ with 86.3% retention of specific capacitance.

INTRODUCTION

Recently, a crucial and challenging topic for scientist is the synthesis and design of novel materials for energy storage device as an alternative to the depleting traditional energy resources like fossil fuels. As a promising future for energy storage systems, supercapacitor also called electrochemical capacitor has attracted great importance due to their unique properties such as long operating lifetimes, high power density, moderated energy density, green environmental protection, in supporting the voltage of a system during enhanced loads, from portable equipment to electric vehicles, *etc.*[1] Based on their energy storage mechanism, supercapacitors are classified into two types: (i) electrochemical double layer capacitor (EDLC) and (ii) pseudocapacitor or redox supercapacitor, involving non-Faradaic and Faradaic processes, respectively.[2] Non-faradaic process does not involve any redox reaction; the energy is stored by the accumulation of the ionic charges on the electrode/electrolyte interfaces. Carbonaceous materials such as activated carbon, carbon nanotube, carbon aerogel, carbon cloth and graphene are the most commonly used materials as electrodes in EDLC.[3-4] In faradaic process, energy is produced by the fast reversible faradaic transitions redox reactions of active materials. Typical effective pseudocapacitive materials consist of transition metal oxides and hydroxide such as MnO_2,[5] $Co(OH)_2$,[6] RuO_2,[7] $Ni(OH)_2$,[8] NiO,[9] and conducting polymers such as polyaniline,[10] polypyrrole,[11] and polythiophene.[12] Among the transition metal oxides, RuO_2 gives very high specific capacitance but still it is not used commercially due to less availability and very high cost. However, the future growth in the field of supercapacitor is based on the two approaches: either to develop a new material through the methods of solid state chemistry/materials science or to improve the micro-structure of existing materials. Additionally, binary metal oxides such as $NiMoO_4$,[13] $CoMoO_4$,[14] and $MnMoO_4$,[15] have fascinated great research interest in recent days due to their feasible variable oxidation states and comparative higher electrical conductivity. Liu *et al.*[14] reported a specific capacitance of 326 F/g for hydrothermally synthesized one dimensional $CoMoO_4{\cdot}0.9H_2O$ nanorods at a current density of 5 mA cm^{-1}. To improve the performance of $CoMoO_4$ various efforts have been devoted such as incorporation of carbonaceous materials like MWCNT[16] or Graphene.[17] Xu *et al*. obtained a specific capacitance of 170 F/g for microwave synthesized $CoMoO_4$/MWCNTs at a current density of 0.1 A/g.[16] Whereas, Xia *et al.* achieved a specific capacitance of about 394.5 F/g at the scan rate of 1 mV/s for hydrothermally synthesized $CoMoO_4$/Graphene composites.[17]

Polyaniline (PANI), a unique conjugated polymer has been extensively studied as a promising material for energy storage and conversion with its high conductivity, exhibiting a fast reversible faradaic reaction, excellent pseudocapacitive behavior and low cost combining with the easiness of synthesis.[18] The major problem with the virgin electrode of PANI is poor cycling stability as the active redox site of polymer backbone is demolished after within a limited number of charge-discharge cycles. Therefore, to increase the cyclic stability, PANI is often used as a hybrid material with metal oxide/sulfide or carbonaceous material such as graphene, carbon nanotube, *etc*.[19-22]

In our present work we have demonstrated an in-situ oxidative polymerization method for the preparation of nanodimentional amorphous polyaniline coated 1D $CoMoO_4{\cdot}0.75H_2O$ nanorods for supercapacitor energy storage application. The composite material can be effectively handled within a larger potential range exhibiting high energy density at a high power delivery rate. The synthesis, physical and electrochemical characterizations are discussed in detailed.

MATERIALS AND METHOD

All materials were used prior to further purification. Aniline (99.5%) monomer, ammonium persulphate (APS) were purchased from Merck chemicals, India. Carbon black, polyvinylidine difluoride (PVDF), sodium molybdate (Na_2MoO_4) was purchased from Sigma Aldrich Ltd., Germany. Cobalt chloride hexahydrate ($CoCl_2.6H_2O$) and ethanol were procured from Loba Chemie, India. All chemicals were used in this research were of analytical grade and doubly distilled water was used throughout the experiment. All of the aqueous solutions were prepared with double distilled water.

PREPARATION OF $CoMoO_4.0.75H_2O$

For the preparation of $CoMoO_4{\cdot}0.75H_2O$, we used a facile hydrothermal method. In a typical synthesis procedure, 20 ml 0.1 M $CoCl_2.6H_2O$ solution was mixed with 20 ml 0.1 M sodium molybdate (Na_2MoO_4) slowly with continuous stirring. The mixture was then transferred into a 50 ml capacity Teflon sealed autoclave and heated in a muffle furnace at 180 °C for 16 h. A violet precipitate was obtained. The precipitates were centrifuged and washed with a water–ethanol mixture several times and dried at 60 °C. The as prepared sample was labeled as $CoMoO_4{\cdot}0.75H_2O$.

PREPARATION OF $CoMoO_4.0.75H_2O$/PANI COMPOSITE

For the preparation of $CoMoO_4{\cdot}0.75H_2O$/PANI composite an *in situ* oxidative polymerization process was followed, where ammonium persulfate was used as oxidant. A total of three reactions set was prepared by varying the concentration of aniline monomer and the APS keeping the amount of $CoMoO_4{\cdot}0.75H_2O$ constant. Briefly, the aniline monomer was well dispersed in 100 ml ice water by ultrasonication for 5 minutes. Then 150 mg of prepared $CoMoO_4{\cdot}0.75H_2O$ was added to it and stirred for two minutes at a low r.p.m. APS was dissolved in 100 ml ice water and the solution was poured drop by drop to the above suspension of prepared $CoMoO_4{\cdot}0.75H_2O$ containing aniline monomer while continuous stirring at 250 r.p.m. and the stirring was continued to 3h. The temperature of the bulk material was kept at 0 - 5 °C during the whole stirring process. Then the whole material was kept in refrigerator overnight and then washed with water ethanol several times and the final precipitation was dried at 60°C. The amount of APS used were 0.5 g, 1 g and 1.5 g, respectively, for 0.1 ml, 0.2 ml and 0.3 ml aniline monomer and the prepared materials were labeled as $CoMoO_4{\cdot}0.75H_2O$/PANI (0.1), $CoMoO_4{\cdot}0.75H_2O$/PANI (0.2), and $CoMoO_4{\cdot}0.75H_2O$/PANI (0.3). Pure PANI was prepared by using 0.2 ml aniline monomer and 1 g APS as oxidant.

RESULTS AND DISCUSSIONS

Materials characterizations

X-RAY DIFFRACTION ANALYSIS

X-ray diffraction (XRD) analysis was carried out by Rigaku ULTIMA-III X-ray diffractometer, with Cu Kα radiation (λ = 1.5418 Å). The XRD pattern of the as prepared virgin $CoMoO_4{\cdot}0.75H_2O$ and $CoMoO_4{\cdot}0.75H_2O$/PANI composite is shown in Figure 1. For $CoMoO_4{\cdot}0.75H_2O$, the peaks are well matched with the JCPDS number 04-011-8282. Peaks at 2θ = 9.68, 13.3, 17.15, 20.9, 23.42, 26.55, 29.68, 33.06, 39.8, 42.72, 43.66, 49.68, 51.61, 52.9 and 61.25 degrees indicate the (001), (100), (-101), (-1-11), (102), (121), (003), (-103), (310), (-301), (230), (-204), (034), (141) and (006) planes, respectively.[23] The XRD pattern of PANI, the characteristic peaks appeared at 14.4, 20.34 and 25.5, corresponding to (011), (020) and (200) crystal planes of PANI.[24] The XRD pattern of the binary composite, only characteristic peaks of PANI can be observed indicating successful coating of the amorphous PANI over the $CoMoO_4{\cdot}0.75H_2O$.

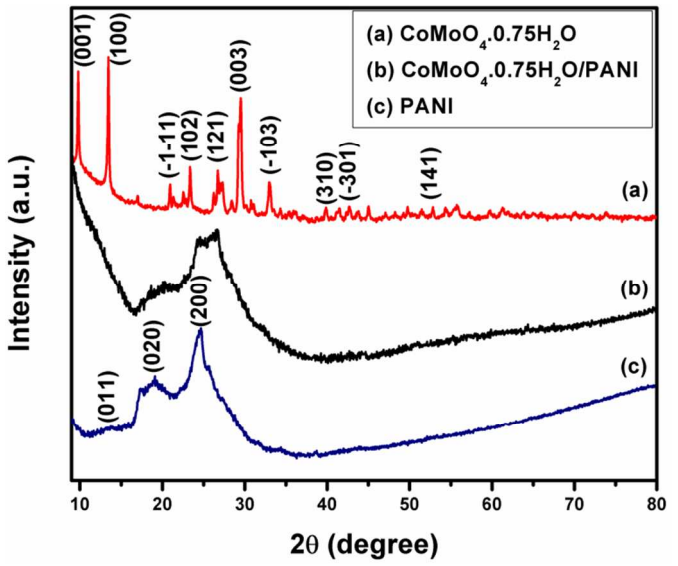

Figure 1. XRD pattern of the as synthesized $CoMoO_4.0.75H_2O$ (a), $CoMoO_4.0.75H_2O$/PANI (b), and pure PANI(c).

FTIR ANALYSIS

Fourier transform infrared spectroscopy (FTIR) was performed by NEXUS 870 FT-IR (Thermo Nicolet) instrument. The FTIR spectra of $CoMoO_4{\cdot}0.75H_2O$, $CoMoO_4{\cdot}0.75H_2O$/PANI and pure PANI are shown in Figure 2a and 2b. It is found that the FTIR absorption of $CoMoO_4{\cdot}0.75H_2O$ between 951 cm^{-1} and 728 cm^{-1} are ascribed to the Mo–O stretching bands. The low frequency peak at 433 cm^{-1} indicates vibrations due to the Co and Mo building blocks of $CoMoO_4$.[25] The asymmetric stretching modes of MoO_4 are about 1606 cm^{-1}. Absorption at 3400~3250 cm^{-1} is attributed to the typical OH stretching bands. The absorption peaks are clearly shown in the Figure 2b. In the case of PANI the peaks are well matched with the literature. The peaks at 1568 cm^{-1} and 1490 cm^{-1} are attributed to the C=C stretching of quinonoid rings and C=C stretching of benzenoid rings, respectively. The absorption peak at 1291 cm^{-1} corresponding for the C-N stretching.[26] The band at 3400 cm^{-1} indicates the stretching of N-H band of aromatic ring in PANI and $CoMoO_4{\cdot}0.75H_2O$/PANI. The peaks at 1112 cm^{-1} and 802 cm^{-1} are attributed to the characteristic of C-N=C bond stretching,[27] and out-of-plane bending vibration of C-H bond in benzene rings.[26] For $CoMoO_4{\cdot}0.75H_2O$/PANI composite, all the absorption peaks are similar to the absorption peaks of PANI except the peak at 951cm^{-1} for the Mo–O stretching which is shifted to the right side with little extent in composite, suggesting the surface of the composite is composed with PANI.[28]

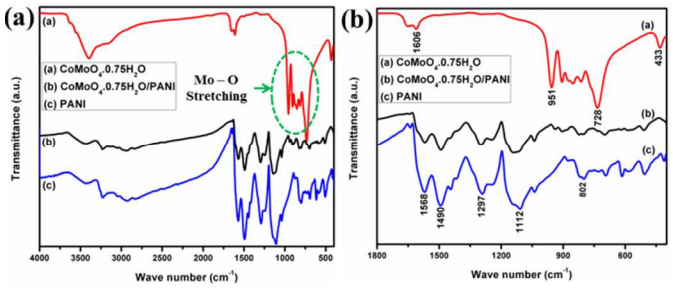

Figure 2. FTIR spectrum of $CoMoO_4.0.75H_2O$, $CoMoO_4.0.75H_2O$/PANI and pure PANI (a); enlarged FTIR spectrum of $CoMoO_4.0.75H_2O$, $CoMoO_4.0.75H_2O$/PANI and pure PANI (b).

MORPHOLOGICAL ANALYSIS

The morphological analysis of the materials was performed in terms of FESEM and TEM analysis and the images are shown in Figure 3 and 4, respectively. Figure 3a and 3b shows FESEM images of the $CoMoO_4{\cdot}0.75H_2O$ nanorods at various magnifications, revealing its average diameter of 200–500 nm with an average length of 2–5 µm. The FESEM images of the binary composites using different concentrations of aniline monomer of 0.1 ml, 0.2 ml and 0.3 ml are shown in Figure 3c, 3d and 3f, respectively. The FESEM image of the binary composites prepared using 0.1 ml aniline monomer indicate the presence of nanospherical PANI coated over the $CoMoO_4$ nanorods. However, non uniform coating of PANI was observed due to the presence of the low amount of PANI. The surface morphology of the $CoMoO_4{\cdot}0.75H_2O$/PANI composite using 0.2 ml aniline exhibits that the nanorods architecture of the $CoMoO_4{\cdot}0.75H_2O$ is almost buried under the PANI (Figure 3d) and the individual $CoMoO_4{\cdot}0.75H_2O$ nano rod was hardly found. This indicates excellent coating on the nanorods by the amorphous PANI. Figure 3e shows the higher magnification image of the composite revealing the sphere like morphology of the PANI in the bulk. Figure 3f indicates that the size of the PANI spheres increases with increasing the amount of PANI from 0.2 ml to 0.3 ml. The elemental mapping of the $CoMoO_4{\cdot}0.75H_2O$/PANI composite prepared using 0.2 ml aniline is shown in Figure S1 (see supporting information), which indicates the presence of Co, Mo, and O for $CoMoO_4{\cdot}0.75H_2O$ and as well as C and N for PANI in the $CoMoO_4{\cdot}0.75H_2O$/PANI composite. The corresponding weight and atomic percentage of the elements are shown in Figure S2. The EDX ananlysis also confirms the successful formation of the $CoMoO_4{\cdot}0.75H_2O$/PANI composite where the nanorods are buried up under the PANI.

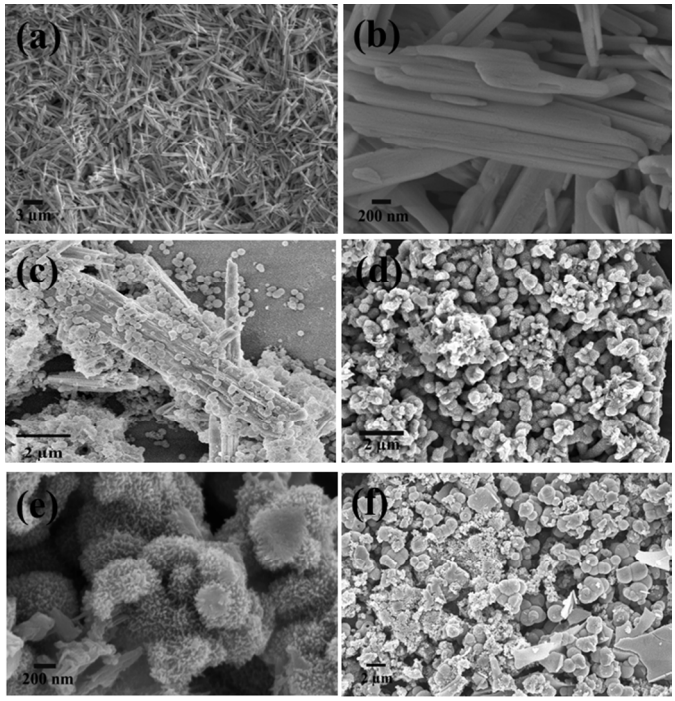

Figure 3. FESEM images of $CoMoO_4.0.75H_2O$ nanorods at low magnification (a), and at high magnification (b); FESEM images of $CoMoO_4.0.75H_2O$/PANI composites prepared using 0.1 ml (c), 0.2 ml (d), and 0.3 ml (f) aniline monomer; High magnification FESEM image of the $CoMoO_4.0.75H_2O$/PANI composite by using 0.2 ml aniline monomer (e).

The TEM image (Figure 4a) of the $CoMoO_4{\cdot}0.75H_2O$ also suggests its rod like morphology and the corresponding SAED pattern indicates its single crystalline nature (Figure 4b). Figure 4c and 4d are the TEM images of the $CoMoO_4{\cdot}0.75H_2O$/PANI composite prepared using 0.2 ml PANI at low and high magnifications, respectively. These images also support the FESEM analysis. In case of the binary composite two types of PANI morphology can be seen, amorphous nanodimentional PANI uniformly coated on $CoMoO_4{\cdot}0.75H_2O$ nanorod and interconnected hollow sphere like PANI (Figure 4e) with dimension of about 0.8-1 µm diameter inside the bulk material.

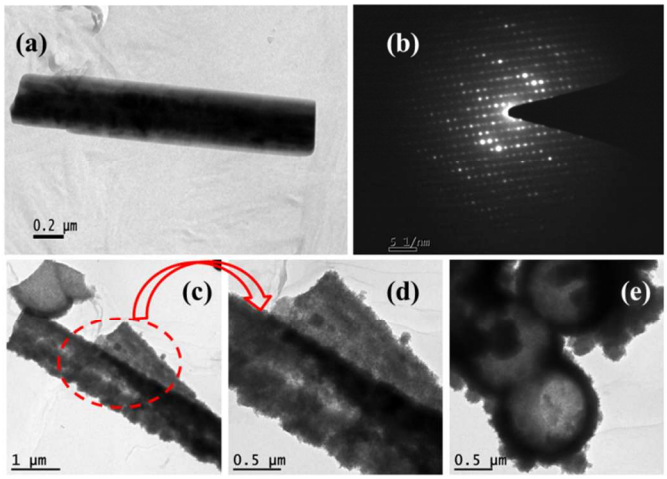

Figure 4. TEM image of $CoMoO_4.0.75H_2O$ nanorod (a) with the corresponding SAED pattern (b). TEM images of CoMoO4.0.75H2O/PANI (0.2) composite with low magnification (c) and with high magnification (d). The interconnected hollow spheres of PANI in $CoMoO_4.0.75H_2O$/PANI bulk composite (e).

Electrochemical characterizations

For the electrochemical measurements we used a three electrode system, where active materials fabricated on nickel foam (1 cm x 1 cm), Pt electrode and saturated calomel electrode were chosen as working electrode, counter electrode and a reference electrode, respectively. For the preparation of working electrode, active materials, carbon black and polyvinylidine fluoride (PVDF) were taken in N-Methyl-2-pyrrolidone (NMP) with the ratio of 8:1:1. The prepared paste was cast onto nickel foam and allowed to dry fully under air. The electrochemical tests, galvanostatic charge-discharge (GCD) and cyclic voltammetry (CV) techniques were performed by using Biologic SP-150 instrument in an aqueous 1M Na_2SO_4 electrolyte.

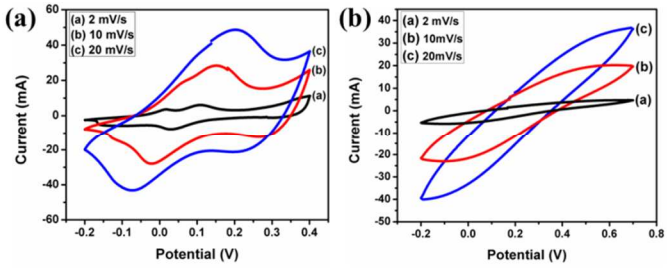

Figure 5. Cyclic voltammetry curves of $CoMoO_4.0.75H_2O$ (a) and pure PANI (b) at different scan rates of 2, 10 and 20 mV/s.

Figure 5a and 5b demonstrates the cyclic voltammetry plots of virgin $CoMoO_4.0.75H_2O$ nanorod and pure PANI at different scan rates of 2, 10 and 20 mV s^{-1}, respectively. The CV plots of virgin $CoMoO_4.0.75H_2O$ are having a pair of redox peaks during the positive and negative sweep suggesting that the specific capacitance comes from the redox mechanism. The faradaic reactions corresponding the redox peaks are attributed to the redox reaction of Co(II)/Co(III).[29] The well-defined redox peaks at a high scan rate (20 mV/s) indicate that the materials have the properties of high rate capability and good reversibility.

The specific capacitance (C_S in F/g) of the materials from the CV measurement can be calculated by using the following equation.

$$\text{Specific capacitance } (C_S) = \frac{\int_{V2}^{V1} i(V)dV}{(V2-V1)\nu m}$$

where, i (A) is the instantaneous current in cyclic voltammogram, ν is the potential scan rate (V/s). V1 and V2 are the switching potential, m is the mass of the active material, and $\int_{V2}^{V1} i(V)dV$ determines the area of the I-V curve.

The highest specific capacitance of $CoMoO_4.0.75H_2O$ and pure PANI are 373 F/g and 306 F/g at a scan rate of 2 mV/s, respectively.

Table 1: Specific capacitance (F/g) of $CoMoO_4.0.75H_2O$ and pure PANI from CV curves

Scan rates	2 mV/s	10 mV/s	20 mV/s
sp. cap. (F/g) of $CoMoO_4.0.75H_2O$	373	287	254
sp. cap. (F/g) of pure PANI	306	256	212

The $CoMoO_4.0.75H_2O$/PANI composite shows the more symmetric and high area curve due to increasing conductivity and pseudocapacitive properties in the presence of conducting polymer PANI. At different scan rates, there is no peak in the CV curves, implying that the electrode material is charged and discharged at a pseudo-constant rate over the complete voltammetric cycle. With increasing the scan rate the redox current increases, the anodic peak shifted towards positive potential and the cathodic peak shifted towards negative potential. The current response with the scan rate indicates that the interfacial faradaic redox reactions and the rates of electronic/ionic transportations.[29]

To understand the optimum content ratio of $CoMoO_4.0.75H_2O$ nanorod to aniline monomer in the composite for the best electrochemical behaviour, cyclic voltammetry analysis of all three $CoMoO_4.0.75H_2O$/PANI composites were carried out at different scan rates of 2, 10 and 20 mV/s and the plots are shown in the Figure 6. Amongst the three composites, the maximum specific capacitance of 475 F/g, is exhibited by $CoMoO_4.0.75H_2O$/PANI (0.2). This specific capacitance value is much more higher than the specific capacitance of 394.5 F/g at a scan rate of 2 mV/s for $CoMoO_4$/graphene composites, reported by Xia *et al.*[17] Padmanathan *et al.*[30] reported the specific capacitance of 450.2 F/g and 333.3 F/g for the hybrid $CoMoO_4$/Carbon and $CoMoO_4$/reduced graphene oxide nanorods at scan rate of 2mV/s which is lower than the $CoMoO_4.0.75H_2O$/PANI (0.2) composites. With the increasing scan rates specific capacitance of the electrode material decreases due to slow redox reaction at a high scan rate. The $CoMoO_4.0.75H_2O$/PANI composite using 0.2 ml aniline monomer shows the maximum specific capacitance amongst the three. The synergistic combination of both metal oxide and polyaniline plays a crucial role in the enhancement of specific

capacitance for $CoMoO_4.0.75H_2O$/PANI (0.2 ml) as compared to other composites. It serves the more redox active sites of polyaniline and metal oxide. This optimum aniline monomer (0.2 ml) leads to more accessibility of electrolyte which ensures the better accumulation charge and more ions insertion/deinsertion of ions into/out of the composites during charging/discharging. In case of other composite like $CoMoO_4.0.75H_2O$/PANI (0.1 ml), PANI unit could not cover all over the metal oxide homogeneously which serves less redox active sites as compared with $CoMoO_4.0.75H_2O$/PANI (0.2 ml). On the other hand, PANI unit for $CoMoO_4.0.75H_2O$/PANI (0.3 ml) are more densely attached with metal oxide so that the electrolyte can not penetrate the metal oxide wall, i.e. metal oxide can not take part in the redox reaction resulting low specific capacitance. Also, sharp current drop between +0.1 to -0.2 V is not the desirable CV behaviour of the supercapacitor materials. The cyclic voltammetry curves of $CoMoO_4.0.75H_2O$/PANI composites at different concentration of aniline monomer 0.1 ml, 0.2 ml, 0.3 ml and pure PANI at a scan rate of 2 mV/s are shown in Figure 8a.

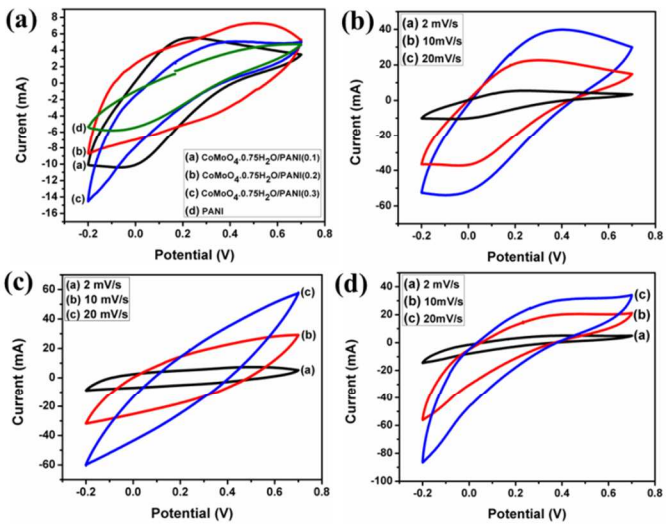

Figure 6. Cyclic voltammetry curves of pure PANI and different $CoMoO_4.0.75H_2O$/PANI composites at a scan rate of 2mV/s (a). Cyclic voltammetry curves of $CoMoO_4.0.75H_2O$/PANI composites at different concentration of aniline monomer 0.1 ml (b), 0.2 ml (c) and 0.3 ml (d) at different scan rate of 2, 10 and 20 mV/s.

Table 2: Specific capacitance (F/g) of $CoMoO_4.0.75H_2O$/PANI composites prepared using 0.1 ml, 0.2 ml, and 0.3 ml aniline monomer from CV curves

Scan rates	2 mV/s	10 mV/s	20 mV/s
sp. cap. (F/g) of $CoMoO_4.0.75H_2O$/PANI (0.1)	459	361	284
sp. cap. (F/g) of $CoMoO_4.0.75H_2O$/PANI (0.2	475	380	303
sp. cap. (F/g) of $CoMoO_4.0.75H_2O$/PANI (0.3)	442	349	267

As the $CoMoO_4.0.75H_2O$/PANI composite, prepared by using 0.2 ml aniline monomer shows the highest specific capacitance from CV, so the other electrochemical characterizations, such as, galvanostatic charge-discharge measurements and electrochemical impedance spectroscopy study were carried out using $CoMoO_4.0.75H_2O$/PANI (0.2) composite.

In order to investigate the current–voltage behavior of the $CoMoO_4.0.75H_2O$ and $CoMoO_4.0.75H_2O$/PANI composite materials, the coulombic efficiency was first measured to fix the appropriate potential window for these materials. It was decided potential window (-0.2 to 0.4 V) for the virgin $CoMoO_4.0.75H_2O$ and (-0.2 to 0.7 V) for the $CoMoO_4.0.75H_2O$/PANI composite to get the best working efficiency. Coulombic efficiency was calculated from galvanostatic charge-discharge experiments as follows

$$\text{Coulombic efficiency } (\eta) = \frac{\Delta tD}{\Delta tC} \times 100\%$$

where, ΔtC and ΔtD are the times of charging and discharging, respectively. The coulombic efficiency was calculated from the first charge-discharge cycle of $CoMoO_4.0.75H_2O$ and $CoMoO_4.0.75H_2O$/PANI composite at 1 A/g current density about 95% and 113% respectively.

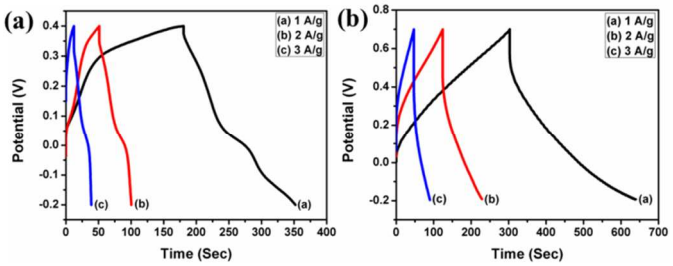

Figure 7. Galvanostatic charge-discharge curves of $CoMoO_4.0.75H_2O$ (a) and $CoMoO_4.0.75H_2O$/PANI (b) at different current density of 1, 2 and 3 A/g.

Galvanostatic charge-discharge (GCD) curves of $CoMoO_4.0.75H_2O$ and $CoMoO_4.0.75H_2O$/PANI composites at various current densities of 1 A/g, 2 A/g and 3 A/g are shown in Figure 7c and 7d. The semi-symmetric GCD curves for both the materials reveal their pseudocapacitive behavior. Incorporation of PANI increases the charging-discharging time in the case of $CoMoO_4.0.75H_2O$/PANI composites.

The specific capacitance (C_{sp}) was calculated from the equation below

$$\text{Specific capacitance, } C_{sp} = \frac{i \times \Delta t}{m \times \Delta v}$$

where, i, m, Δt and Δv is the applied current (A), mass (g) of the active material, discharge time and potential window, respectively. The highest specific capacitances of $CoMoO_4.0.75H_2O$ and $CoMoO_4.0.75H_2O$/PANI composites are obtained at 1 A/g current density of 285 F/g and 380 F/g, respectively. Highly conductive polymer PANI plays the vital role to increase the specific capacitance in case of $CoMoO_4.0.75H_2O$/PANI composite. With the increase of current density, the specific capacitance gradually decreases because of lower diffusion of electrolyte into the inner surface of the active material which results in the incomplete insertion reaction. Table 3 represents the specific capacitance of $CoMoO_4.0.75H_2O$ and $CoMoO_4.0.75H_2O$/PANI composites from GCD curves at various current densities.

Table 3: Specific capacitance (F/g) of $CoMoO_4 \cdot 0.75H_2O$ and $CoMoO_4 \cdot 0.75H_2O$/PANI composites from charge-discharge measurements

Current densities	1 A/g	2 A/g	3 A/g
sp. cap. (F/g) of $CoMoO_4 \cdot 0.75H_2O$	285	163	133
sp. cap. (F/g) of $CoMoO_4 \cdot 0.75H_2O$/PANI	380	237	213

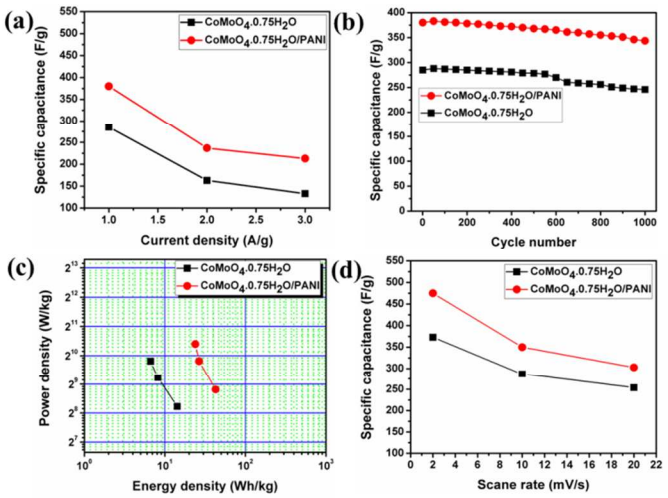

Figure 8. Variation of Specific capacitance as a function of current density (a), cycle number (b) and scan rate (d) of $CoMoO_4 \cdot 0.75H_2O$ and $CoMoO_4 \cdot 0.75H_2O$/PANI composite. Ragone plot of $CoMoO_4 \cdot 0.75H_2O$ and $CoMoO_4 \cdot 0.75H_2O$/PANI composite (c).

Energy density and Power density decide the fate of a material to behave as electrode material for supercapacitor application. Energy densities and power densities of the materials were calculated by the following equations

$$\text{Energy density (E)} = \frac{1}{2} C_{sp} (\Delta V)^2$$

$$\text{Power density (P)} = \frac{E}{T}$$

where, C_{sp} = specific capacitance in F/g, and ΔV = potential window in volt, T is the discharge time of the charge-discharge curves from where the specific capacitance was calculated. Figure 8c shows the energy density versus power density curve in terms of Ragone plot. The highest energy density of 14.25 Wh/kg and 42.7 Wh/kg were achieved by the virgin $CoMoO_4 \cdot 0.75H_2O$ and $CoMoO_4 \cdot 0.75H_2O$/PANI composite at a power density of 300 W/kg and 450 W/kg, respectively. The $CoMoO_4 \cdot 0.75H_2O$ and $CoMoO_4 \cdot 0.75H_2O$/PANI composite show the comparable value of energy density and power density with some other similar composites, such as, PANI-metal oxide and graphene-metal oxide composites. Zou *et al.*[31] and Hu *et al.*[32] reported the energy density of 33.6 Wh/kg and 42.4 Wh/kg for WO_3/PANI and PANI/SnO_2 comoposites, respectively. Jaidev *et al.*[19] shown maximum energy density of 17.8 Wh/kg for the PANI/MnO_2 hybrid nanocomposite. Xia *et al.*[17] acheived highest energy density of 54.8 Wh/kg at a power density of 197.2 W/kg for the $CoMoO_4$/Graphene composite, which is higher than that of pure-$CoMoO_4$ (10.0 Wh/kg at a power density of 36.0 W/kg) at 1 mV/s scan rate. Ghosh *et al.*[13] reported the energy density of 4.444 and 10.833 Wh/kg for $NiMoO_4.nH_2O$ and Graphene-$NiMoO_4.nH_2O$ composite at a same power density of 1250 W/kg. The variation of energy density and power density with the current densities of both the materials are shown in Table 4. To determine the cycle stability GCD was performed up to 1000 cycles at a current density of 1 A/g. The cycle stability of the $CoMoO_4 \cdot 0.75H_2O$ and $CoMoO_4 \cdot 0.75H_2O$/PANI composites are demonstrated in Figure 8b. The retention of the specific capacitance of $CoMoO_4 \cdot 0.75H_2O$ and $CoMoO_4 \cdot 0.75H_2O$/PANI composites are 86.3% and 90.4%, respectively. The composite shows higher retention of specific capacitance than the virgin electrode due to the synergistic effect between pure $CoMoO_4 \cdot 0.75H_2O$ and PANI. The low cycle stability of $CoMoO_4 \cdot 0.75H_2O$ can be explained by the swelling of the electrode materials through the faradaic reactions. In case of the composites, the retention of the specific capacitance only 4.1% higher than the virgin $CoMoO_4 \cdot 0.75H_2O$, this can be explained by considering the deterioration of PANI after several shrinking and swelling charge discharge cycles.

Table 4: Calculated energy density (Wh/kg) and power density (W/kg) from charge-discharge measurements

Current densities	1 A/g	2 A/g	3 A/g
Energy density (Wh/kg) of $CoMoO_4 \cdot 0.75H_2O$	14.25	8.2	6.65
Power density (W/kg) of $CoMoO_4 \cdot 0.75H_2O$	300	600	900
Energy density (Wh/kg) of $CoMoO_4 \cdot 0.75H_2O$/PANI	42.7	26.6	23.87
Power density (W/kg) of $CoMoO_4 \cdot 0.75H_2O$/PANI	450	900	1350

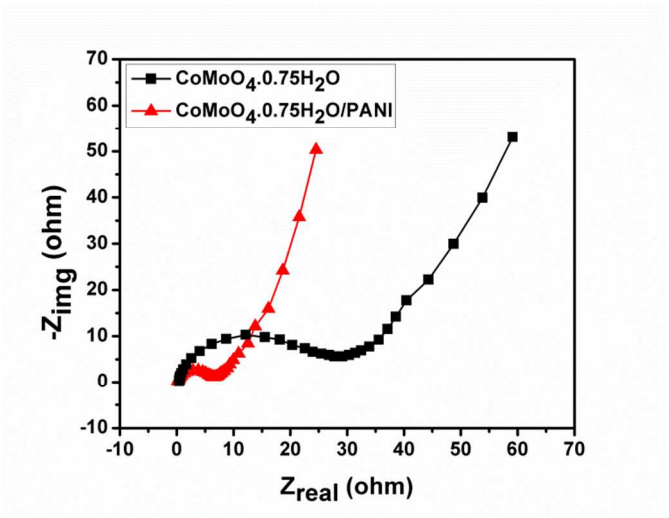

Figure 9. Nyquist plots of pure $CoMoO_4.0.75H_2O$ and $CoMoO_4.0.75H_2O$/PANI composite.

To measure the efficiency of the electrode material electrochemical impedance spectroscopy (EIS) study was performed within the frequency range of 100 kHz to 10 mHz. Figure 9 demonstrated the EIS of the pure $CoMoO_4.0.75H_2O$ and $CoMoO_4.0.75H_2O$/PANI composite. The EIS has been represented in terms of Nyquist plot which gives the electrochemical information, such as charge transfer resistance, solution resistance, *etc.* The diameter of the semicircle

represents charge transfer electrochemical reaction resistance, also known as faradaic resistance and determines the rate of response of the electrode material in particular electrolyte. From the Figure 9 it can be found that the semicircle diameter of virgin $CoMoO_4.0.75H_2O$ (28 ohm) is higher than the diameter of the semicircle of composite (6 ohm), suggesting the virgin $CoMoO_4.0.75H_2O$ exhibits high resistance/low conductivity than the composites. These results indicate, $CoMoO_4.0.75H_2O$/PANI composite is more potential candidate as an electrode material for supercapacitor applications rather than virgin $CoMoO_4.0.75H_2O$.

Conclusions

In conclusion, the virgin $CoMoO_4{\cdot}0.75H_2O$ and $CoMoO_4{\cdot}0.75H_2O$/PANI composites by using different concentration of aniline monomer were successfully synthesized by hydrothermal and *in situ* oxidative polymerization method. Due to the presence of variable oxidation state of the metal forming the metal molybdate compound it can effectively behave as pseudocapacitive electrode material. A maximum specific capacitance of 285 F/g was achieved at 1 A/g current density accompanied with high energy density of 14.25 Wh/kg at a power delivery rate of 300 W/kg. The synergistic interaction of the PANI with $CoMoO_4$ resulted in an increased specific capacitance of 380 F/g and the larger working potential resulted in an elevated energy density of 42.7 Wh/kg at high power density of 450 W/kg accompanied with high cycle life. The reasonable high value of energy density and power density along with the excellent cycling stability makes the $CoMoO_4{\cdot}0.75H_2O$/PANI composite an efficient supercapacitor electrode material.

Acknowledgements
The authors thank IIT Kharagpur, India for financial support and instrumental help. Autors are also thankful to Miss. Krishna Chattopadhyay, IIT Kharagpur, India, for XRD analysis.

Notes and references
[a] Materials Science Centre, Indian Institute of Technology Kharagpur, Kharagpur – 721302, India. Email: chapal12@yahoo.co.in
[b] Sustainable Energy Technologies (SET) Centre, College of Engineering, King Saud University, PO Box 800, Riyadh 11421, Kingdom of Saudi Arabia.
Electronic Supplementary Information (ESI) available: [EDX and elemental mapping of CoMoO4.0.75H2O composite by using 0.2 ml aniline monomer.]. See DOI: 10.1039/b000000x/

References

1 M. Zhu, C.J. Weber, Y. Yang, M. Konuma, U. Starke, K. Kern, and A.M. Bittner, *Carbon,* 2008, **46**, 1829-1840.
2 B. Conway, Electrochemical Supercapacitors, Kluwer Academic/Plenum Publishers, New York, 2nd edn, 1999.
3 L. L. Zhang and X. S. Zhao, *Chem. Soc. Rev.*, 2009, **38**, 2520-2531.
4 Y. B. Tan and J.-M. Lee, *J. Mater. Chem. A*, 2013, **1**, 14814-14843.
5 B. Ming, J. Li, F. Kang, G. Pang, Y. Zhang, L. Chen, J. Xu, and X. Wang, *Journal of Power Sources* 2012, **198**, 428-431.
6 D. Ghosh, S. Giri and C. K. Das, *ACS Sustainable Chem. Eng*. 2013, **1**, 1135-1142.
7 V. Subramanian, S. C. Hall, P. H. Smith and B. Rambabu, *Solid State Ionics*, 2004, **175**, 511-515.
8 D. Ghosh, S. Giri, A. Mandal and C. K. Das, *Chemical Physics Letters*, 2013, **573**, 41-47.
9 C. Yuan, X. Zhang, L. Su, B. Gao and L. Shen, *J. Mater. Chem*., 2009, **19**, 5772-5777.
10 D. Ghosh, S. Giri, A. Mandal and C. K. Das, *Applied Surface Science*, 2013, **276**, 120-128.
11 L.-Z. Fan and J. Maier, *Electrochemistry Communications*, 2006, **8**, 937-940.
12 A. Laforgue, P. Simon, C. Sarrazin and J.-F. Fauvarque, *Journal of Power Sources*, 1999, **80**, 142-148.
13 D. Ghosh, S. Giri and C. K. Das, *Nanoscale*, 2013, **5**, 10428-10437.
14 M.-C. Liu, L.-B. Kong, X.-J. Ma, C. Lu, X.-M. Li, Y.-C. Luo and L. Kang, *New J. Chem*., 2012, **36**, 1713-1716.
15 K.K. Purushothaman, M. Cuba and G. *Muralidharan, Materials Research Bulletin*, 2012, **47**, 3348-3351.
16 Z. Xu, Z. Li, X. Tan, C. M. B. Holt, L. Zhang, B. S. Amirkhiz and D. Mitlin, *RSC Adv*ances, 2012, **2**, 2753-2755.
17 X. Xia, W. Lei, Q. Hao, W. Wang and X. Wang, *Electrochimica Acta*, 2013**, 99**, 253-261.
18 H. Mi, X. Zhang, S. Yang, X. Ye and J. Luo, *Materials Chemistry and Physics*, 2008, **112**, 127-131.
19 Jaidev, R. I. Jafri, A. K. Mishra and S. Ramaprabhu, *J. Mater. Chem*., 2011, **21**, 17601.
20. K.-J. Huang, L. Wang, Y.-J. Liu, H.-B. Wang, Y.-M. Liu and L.-L. Wang, *Electrochimica Acta*, 2013, **109**, 587-594.
21 Q. Wu, Y. Xu, Z. Yao, A Liu and G. Shi, *ACS Nano*, 2010, **4**, 1963-1970.
22 V. Gupta and N. Miura, *Electrochimica Acta,* 2006*,* **52,** 1721-1726.
23 K. Eda, Y. Uno, N. Nagai, N. Sotani and M. S. Whittingham, *Journal of Solid State Chemistry*, 2005, **178**, 2791-2797.
24 L. Ding, Q. Li, D. Zhou, H. Cui, H. An and J. Zhai, *Journal of Electroanalytical Chemistry*, 2012, **668**, 44-50.
25 G. Kianpour, M. S.-Niasari and H. Emadi, *Superlattices and Microstructures,* 2013, **58**, 120-129.
26 C. Li, J. Wang, Y. Wen, Y. Ning, Y. Wen, X. Yuan, M. Li and D. Yang, *ECS Electrochemistry Letters*, 2013, **2** (1), H1-H4.
27 B. Kavitha, K. Prabakar, K. S. kumar, D. Srinivasu, Ch. Srinivas, V.K.Aswal, V. Siriguri and N. Narsimlu, *IOSR Journal of Applied Chemistry* 2012, **2**, 16-19.
28 S. Kumar and S. Jain, *Journal of Chemistry*, 2014, Article ID 837682, doi:10.1155/2014/837682.
29 L.-Q. Mai, F. Yang, Y.-L. Zhao, X. Xu, L. Xu and Y.-Z. Luo, *Nat. Commun.*, 2011, **2**, 381-385.
30 N. Padmanathan, K. M. Razeeb and S. Selladurai, *Ionics,* 2014, DOI 10.1007/s11581-014-1089-0.
31 B.-X. Zou, Y. Liang, X.-X. Liu, D. Diamond, K.-T. Lau, *Journal of Power Sources*, 2011, **196**, 4842-4848.
32 Z.-A. Hu, Y.-L. Xie, Y.-X. Wang, L.-P. Mo, Y.-Y. Yang, Z.-Y. Zhang, *Materials Chemistry and Physics*, 2009, **114,** 990.